Identification of *MYCN* non-amplified neuroblastoma subgroups points towards molecular signatures for precision prognosis and therapy stratification

Xiaoxiao Hu[1,2,3#], Yilu Zhou[4,5#], Charlotte Hill[4], Kai Chen[1,3], Cheng Cheng[1,3], Xiaowei Liu[1,3], Peiwen Duan[1,3], Yaoyao Gu[1,3], Yeming Wu[1,3,6], Rob M Ewing[4,5], Zhongrong Li[2], Zhixiang Wu[1,3,6]* and Yihua Wang[4,5]*

1. Department of Paediatric Surgery, Xinhua Hospital, School of Medicine, Shanghai Jiaotong University, Shanghai 200092, China.
2. Department of Paediatric Surgery, The Second Affiliated Hospital and Yuying Children's Hospital of Wenzhou Medical University, Wenzhou 325000, China.
3. Division of Paediatric Oncology, Shanghai Institute of Paediatric Research, Shanghai 200092, China.
4. Biological Sciences, Faculty of Environmental and Life Sciences, University of Southampton, Southampton SO17 1BJ, UK.
5. Institute for Life Sciences, University of Southampton, Southampton SO17 1BJ, UK.
6. Department of Paediatric Surgery, Children's Hospital of Soochow University, Suzhou 215003, China.

[#]These authors contributed equally to this work.

[*]Correspondence should be addressed to YW (e-mail: yihua.wang@soton.ac.uk) or ZW (e-mail: wuzhixiang@xinhuamed.com.cn),

Running title: Molecular subtypes in *MYCN* non-amplified neuroblastomas

Abstract

Background

Despite the extensive study of *MYCN*-amplified neuroblastomas, there is a significant unmet clinical need in *MYCN* non-amplified cases. In particular, the extent of heterogeneity within the *MYCN* non-amplified population is unknown.

Methods

A total of 1,566 samples from 16 datasets were identified in Gene Expression Omnibus (GEO) and ArrayExpress. Characterisation of the subtypes was analysed by ConsensusClusterPlus. Independent predictors for subgrouping were constructed from the single sample predictor based on the multiclassPairs package. Findings were verified using immunohistochemistry and CIBERSORTx analysis.

Results

We demonstrate that *MYCN* non-amplified neuroblastomas are heterogeneous and can be classified into 3 subgroups based on their transcriptional signatures. Within these groups, subgroup_2 has the worst prognosis and this group shows a "*MYCN*" signature that is potentially induced by the overexpression of Aurora Kinase A (AURKA); whilst subgroup_3 is characterised by an "inflamed" gene signature. The clinical implications of this subtype classification are significant, as each subtype demonstrates a unique prognosis and vulnerability to investigational therapies. A total of 420 genes were identified as independent subgroup predictors with average balanced accuracy of 0.93 and 0.84 for train and test datasets, respectively.

Conclusion

We propose that transcriptional subtyping may enhance precision prognosis and therapy stratification for patients with *MYCN* non-amplified neuroblastomas.

Introduction

Neuroblastoma is the most common extra-cranial solid tumour in children, representing 6-10% of all childhood cancers[1]. It is an embryonic tumour arising from precursor cells in the sympathetic nervous system and adrenal medulla[2], with a median age of diagnosis of 18 months [3]. It can also be present in the neck, chest, abdomen, or pelvis[4]. Neuroblastoma is a highly heterogeneous disease, with clinical behaviour ranging from spontaneous regression to drug resistance and metastasis ultimately resulting in death[5]. The prognosis of the disease is poor with a 5-year overall survival of approximately 20%, despite more aggressive therapies[6]. As a result, risk stratification and personalised treatment approaches in neuroblastomas are urgently needed.

The International Neuroblastoma Risk Group Staging System (INRGSS) defines the high-risk group to include patients with *MYCN*-amplified tumours and patients > 18 months old with metastatic tumours[7]. N-MYC is a key regulator of transcription, which activates genes that affect cancer development. It is widely involved in various pathological processes of neuroblastoma including cell growth[8], apoptosis[9], differentiation[10], angiogenesis[11], tumour invasion, and metastasis[12].

MYCN amplification was identified as the first independent prognostic factor indicating adverse clinical outcomes in neuroblastomas[13,14], which is observed in approximately 20% of cases[15] and accounts for about 40% of high-risk neuroblastomas[16]. Despite the extensive study of *MYCN*-amplified neuroblastomas, there is a significant unmet clinical need in *MYCN* non-amplified cases. In particular, the extent of heterogeneity within the *MYCN* non-amplified population is unknown.

Here, we investigated whether transcriptional subtyping of *MYCN* non-amplified neuroblastomas can identify molecular subtypes with discrete prognosis and therapeutic vulnerabilities. Our analysis suggested that *MYCN* non-amplified neuroblastomas were heterogeneous and could be classified into 3 subgroups based on their transcriptional profiling. Within them, subgroup 2 had the worst prognosis and this group had a "*MYCN*" signature that was potentially induced by the overexpression of Aurora Kinase A (AURKA); whilst subgroup 3 was accompanied by an "inflamed" gene signature. We propose that transcriptional subtyping may enhance precision prognosis and therapy stratification for patients with *MYCN* non-amplified neuroblastomas.

Results

Characterisation of molecular subtypes in *MYCN* non-amplified neuroblastomas.

Following quality control and eliminating duplicates (Supplementary Figs. 1 and 2; details provided in the Supplementary Methods), a total of 1,566 samples from 16 datasets were identified in GEO (Gene Expression Omnibus) and ArrayExpress, in which 313 cases are with *MYCN* gene amplification (*MYCN*-AMP) and 1,253 cases *MYCN* non-amplified (*MYCN*-normal) (Fig. 1a; Supplementary Table 1). Following the removal of batch effects (Supplementary Fig. 3a), 2 clear clusters corresponding to *MYCN*-AMP and *MYCN*-normal neuroblastomas, respectively, were visualised using principal component analysis (PCA) (Supplementary Fig. 3b). Samples in the *MYCN*-normal group (n = 1,253) were further randomly divided into a train and a test group with a 7:3 ratio, containing 878 and 375 cases, respectively (Fig. 1a).

In an unbiased attempt to identify subtypes within *MYCN* non-amplified neuroblastomas, we applied consensus clustering to both train and test groups based on 5,792 variable genes (top 50% median absolute deviation; Supplementary Table 2). As determined by the relative area under the cumulative distribution function and cluster-consensus scores, the optimal number of distinct clusters was 3 (Fig. 1b; Supplementary Fig. 3c). In total, within the *MYCN* non-amplified group, subgroup 1 (blue), 2 (green) and 3 (purple) accounts for 46%, 30%, and 24%, respectively (Fig. 1c). Cross-cohort analysis using an unsupervised method SubMap[17] (https://www.genepattern.org/modules) confirmed the robustness of this classification (Supplementary Fig. 4a; false discovery rate, FDR < 0.05).

Further clinical characterisation of these subtypes identified key distinguishing features. Patients within subgroup 2 were frequently observed in the advanced neuroblastomas according to the International Neuroblastoma Staging System (INSS) and in those defined as "high risk"[7] (Fig. 2a and b; Supplementary Fig. 4b). We then analysed their overall survival together with *MYCN*-AMP cases. Patients with *MYCN* amplification had the worst prognosis (Fig. 2c and d; Supplementary Fig. 4c). Importantly, there was a high degree of variability for overall survival among *MYCN* non-amplified cases, in which subgroup 2 was associated with a poor prognosis, followed by subgroup 3; while patients within subgroup 1 had the most favourable outcomes. These observations were consistent in both train and test cohorts. In addition, the molecular subtype classification was a strong independent predictor of mortality including in multivariate analysis with the risk classification that uses commonly measured clinical variables to predict mortality in neuroblastomas[7]. Using subgroup 1 as a reference, the

hazard ratio (HR) and 95% confidence interval (CI) for subgroups 2 and 3 were 20.2 (4.8 ~ 85) and 9.2 (2.1 ~ 40), respectively (Fig. 2e). Similar results were obtained using univariate or multivariate cox regression analysis with age and INSS stages in *MYCN* non-amplified neuroblastomas (Supplementary Table 3). A comprehensive multivariate analysis also revealed our subgroups to be independent of genomic features such as 1p, 11q, and 17q (Supplementary Fig. 4d-f)). Impressively, the molecular subtype classification alone outperformed INSS stages (Fig. 2f) and shows a comparable prediction accuracy as the risk classification (Supplementary Fig. 4g).

Overall, subgroup 2 and subgroup 3 (to a lesser extent) were associated with poor survival in *MYCN* non-amplified neuroblastomas, suggesting fundamentally different mechanisms leading to an advanced disease.

Defining molecular features of the 3 subtypes in *MYCN* non-amplified neuroblastomas.

Using the same 5,792 variable genes described above (Supplementary Table 2), we observed clear distinctions among these 3 subtypes in *MYCN* non-amplified neuroblastomas (Fig. 3a; Supplementary Table 4). Intriguingly, subgroup 2 showed a similar signature to *MYCN*-AMP cases (Fig. 3a). This was consistent with the Gene Set Enrichment Analysis (GSEA), showing HALLMARK_MYC_TARGETS_V1 and V2 significantly enriched in subgroup 2 (Fig. 3b; Supplementary Table 5; FDR = 0.0021 and 0.0017, respectively). In contrast, subgroup 3 exhibited an "inflamed" phenotype, with high expression of genes related to IL6_JAK_STAT3_SIGNALING, INFLAMMATORY_RESPONSE, INTERFERON_ALPHA_RESPONSE and INTERFERON _GAMMA_RESPONSE (Fig. 3b; Supplementary Table 5; all FDR values less than 0.05). None of these pathways were enriched in subgroup 1 (Fig. 3b).

The above analysis was extended using weighted gene co-expression network analysis (WGCNA)[18]. Three molecular modules were identified (Supplementary Fig. 5; Supplementary Table 6) and were further used to construct a protein-protein network consisting of 1,393 genes and 4,490 edges (Fig. 3c; confidence score > 0.9). Molecular module MEturquoise, which was significantly correlated with subgroup 2 (Fig. 3d), was enriched for "Mitotic cell cycle process", "HALLMARK G2M CHECKPOINT", and " DNA repair". In subgroup 3, there were 2 molecular modules, MEblue and MEbrown highly involved (Fig. 3d; Supplementary Table 6). Molecular module MEblue was enriched for pathways, including "HALLMARK EPITHELIAL MESENCHYMAL TRANSITION", "TGF-beta receptor signaling pathway", "PI3K-Akt signaling pathway" and " MAPK signaling pathway" whereas " Cytokine-cytokine

receptor interaction", "T cell activation", "B cell-mediated immunity", "Adaptive immune response" and "Innate immune response" were significantly enriched in molecular module MEbrown.

Subgroup 2 shows a "*MYCN*" signature, potentially induced by Aurora Kinase A (AURKA) overexpression.

Our above analysis suggested that mechanisms other than gene amplification induce N-MYC activity in subgroup 2. Indeed, the mRNA level of *MYCN* in subgroup 2 was significantly lower than cases within the *MYCN*-AMP group (Fig. 4a; Supplementary Table 4; $P < 0.0001$). To evaluate N-MYC activity in neuroblastoma samples, a total of 87 genes upregulated by N-MYC were selected to classify its activity[19]. The *MYCN* score for each sample was calculated using single-sample gene set enrichment analysis (ssGSEA) based on this 87-gene expression signature. *MYCN* scores in subgroup 2 were significantly higher than those in subgroups 1 and 3, and were comparable to those in the *MYCN*-AMP group, although slightly lower (Fig. 4b). Moreover, the *MYCN* score was an independent predictor of mortality including in multivariate analysis with the risk classification (Fig. 4c; HR: 3.3; $P < 0.001$).

To investigate the potential mechanism that leads to higher *MYCN* scores in subgroup 2, correlation analysis coupled with protein-protein interactions (PPI) network construction was performed (Fig. 4d; Supplementary Table 7). Among the candidate genes, *AURKA* (Aurora kinase A) was identified to interact with *MYCN*. AURKA, a serine/threonine kinase regulating the process of mitosis[20], was previously demonstrated to regulate N-MYC protein stability[21]. *AURKA* was expressed at significantly higher levels in subgroup 2 when compared to the other 2 subgroups and its levels were even slightly higher than those in the *MYCN*-AMP group (Fig. 4e). Classifying *MYCN* non-amplified neuroblastomas into high and low groups, we demonstrated that the *AURKA* mRNA levels alone could predict the overall survival (Fig. 4f; HR 4.8; $P < 0.0001$). In addition, the high level of *AURKA* was an independent predictor (HR 3, $P < 0.001$) of mortality including in multivariate analysis with the risk classification (Supplementary Fig. 6).

These findings were further investigated by immunohistochemistry (IHC) staining of N-MYC or AURKA in a custom neuroblastoma tissue microarray, which contains 94 *MYCN* non-amplified neuroblastomas. Within them, 22 samples were positive for N-MYC (Fig. 5a), and they had worse survival compared to those with N-MYC negative staining (n = 72) (Fig. 5b; $P = 0.03$; Supplementary Table 8). In parallel, patients with higher levels of AURKA had unfavourable survival outcomes (Fig. 5c and d; $P = 0.00014$). Moreover, a higher percentage

of patients with high AURKA staining was observed in the N-MYC-positive group compared to the N-MYC-negative group (Fig. 5e; 64% *vs.* 39%; $P = 0.041$).

Taken together, these results suggested that a "*MYCN*" signature in subgroup 2 is potentially induced by AURKA overexpression in *MYCN* non-amplified neuroblastomas.

Subgroup 3 is accompanied by an "inflamed" gene signature.

Considering immune-related pathways were enriched in subgroup 3, the activity of immune cells and pathways were further systematically explored. ssGSEA was performed to calculate enrichment scores of 46 immune gene sets summarised from two previous studies[22,23], and subgroup 3 showed significantly higher activity of immune cells and pathways compared to the other 2 subtypes as well as *MYCN*-AMP group (Fig. 6a; Supplementary Table 9). Consistently, cytolytic activity (CYT) or MHC-1 (major histocompatibility complex-1) scores were highest in subgroup 3 (Fig. 6b and c). This was also true when using the ESTIMATE algorithm to evaluate the immune scores, stromal scores, and tumour purity scores in neuroblastomas[24], showing the highest immune and stromal scores, and lowest tumour purity scores in subgroup 3 (Fig. 6d; Supplementary Fig. 7a and b).

For a comprehensive assessment of immune cell infiltration, we used CIBERSORTx deconvolution[25] to quantify various immune populations based on a single cell RNA sequencing (scRNA-seq) dataset in *MYCN* non-amplified neuroblastoma[26] (Supplementary Fig. 7c). While similar immune cell types were present in each subtype, the absolute number of several immune cell populations were markedly increased in subgroup 3, including B cells, myeloid cells, T cells and pDC (plasmacytoid dendritic cells) (Fig. 6e). Finally, to investigate whether subgroup 3 would benefit more from immunotherapy than the other subgroups, we compared the expression matrix of 3 subgroups with published melanoma datasets including response information after treating with immunotherapies[27,28]. The SubMap analysis highlighted that patients within subgroup 3 are predicted to respond to anti-PD1 immunotherapy (Fig. 6f; Supplementary Fig. 7d). In addition, Su *et al*. observed that anlotinib treatment in neuroblastoma mice reprogrammed the immunosuppressive tumour microenvironment (TME) into an immune-stimulatory TME, leading to an extension in the duration of vascular normalization, and dynamic changes in the expression levels of PD-1 and PD-L1. In addition, it is noteworthy that the combination of anlotinib with PD-1 checkpoint inhibitors counteracted the immune suppression induced by PD-L1 upregulation after monotherapy, ultimately inducing the regression of neuroblastoma[29]. Therefore, we reanalysed

the RNA-seq data of neuroblastoma syngeneic mouse models treated with vehicle/anlotinib for 9 days. Then, we compared the molecular features of each condition to our subgroups. Interestingly, SubMap analysis revealed that subgroup 3 exhibited a significant similarity in expression profile to mouse models after anlotinib treatment (Fig. 6g; $P = 0.032$).

Taken together, these results demonstrated that subgroup 3 is accompanied by an "inflamed" gene signature, and is more likely to benefit from anti-PD1 therapies.

Identification of independent predictors to subgroup patients within *MYCN* non-amplified neuroblastomas

To identify independent predictors for subgrouping, we applied a multi-cohort analysis pipeline via multiclassPairs[30] (see Supplementary Methods). In total, a random forest model, trained using 928 rules derived from a set of 432 genes (Supplementary Table 10) displayed the ability to predict different subgroups accurately in both training and test sets with an F1 score > 0.74 (Supplementary Table 11). The prediction model and example files can be downloaded from https://zenodo.org/records/10258748.

Furthermore, the random forest model successfully stratified patients with *MYCN* non-amplified neuroblastoma into distinct subgroups 1, 2, and 3 with significant differences in survival across five independent validation sets (GSE49711[31], TARGET Microarray[32], TARGET RNA-seq, Westermann ALK cohort[33] and Stefan Hüttelmaier cohort[34] respectively) (Fig. 7a and b; Supplementary Table 11). These independent predictors worked consistently between microarray and RNA-seq within GSE47792 (Fig. 7c).

Evaluation of different patient stratification strategies

Finally, we evaluated our subgrouping method (named Hu_Subgroups) together with other reports. van Groningen and colleagues reported that neuroblastoma is composed of 2 super-enhancer-associated differentiation states: an ‘ADRN’ subgroup showing up-regulated genes involved in adrenergic differentiation and an ‘MES’ subgroup with higher expressions of mesenchymal markers[35]. To quantify these characteristics, we calculated the "ADRN" or "MES" scores of our subgroups based on a 369-gene "ADRN" signature or a 485-gene MES signature, respectively. We observed that subgroup 3 showed the highest "MES" scores and the lowest "ADRN" scores, consistent with our above findings; while subgroups 1 and 2 had the highest "ADRN" scores with the lowest "MES" scores in subgroup 2 (Supplementary Fig. 8a and b).

We also compared Hu_Subgroups with the Valentijn classification[19]. All subgroup 1 samples (n = 33) and two-thirds of subgroup 3 (n = 8) belonged to Valentijn's NEG group, while 13 out of 23 subgroup 2 samples were part of Valentijn's POS group (Fig. 8a; Supplementary Table 12). In addition, the multivariate analysis indicated that our subgroup 3 could be an independent variable after being adjusted by Valentijn's classifier (Fig. 8b).

Since 2006, Oberthuer and colleagues have been dedicated to constructing a molecular classification system capable of accurately categorizing patients into favourable and unfavourable groups, continually iterating over the following decade[36-39]. The most recent molecular predictors NB-th24 and NB-th44 were introduced in 2017[40]. A comparative analysis between our model and their two models reveals a strong consistency in the favourable and unfavourable outcomes of the respective groupings (Fig. 8c). Specifically, 218 out of 230 subgroup 1 samples and 77 out of 124 subgroup 3 samples were labelled as the favourable group based on SVM_th24. Conversely, more than half of the subgroup 2 samples were categorized as unfavourable (Supplementary Table 12). Similar results were identified in the SVM_th44 comparison (Supplementary Fig. 8c). Additionally, multivariate analysis to determine subgroup 2 could serve as an independent variable after adjusting for Oberthuer's classifier (Fig. 8d; Supplementary Fig. 8d).

Recently, Westermann and colleagues reported 4 subgroups in neuroblastoma, including *MYCN*-amplified (MYCN), *MYCN* non-amplified high-risk (MNA-HR), *MYCN* non-amplified low-risk (MNA-LR) and mesenchymal (MES)[41]. With our method, patients within Westermann_MNA-HR can be further classified into 3 subtypes (Fig. 8e), showing different prognosis (Fig. 8f). This was also true for Westermann_MNA-LR (Fig. 8g). A majority of cases in Westermann_MES or MYCN belonged to subgroup 3 and 2, respectively (Fig. 8e).

George and colleagues classified 498 neuroblastoma samples into 4 distinct clusters based on RNA-seq profiles[42]. These clusters include the George_Hi-MYCN cluster, characterized by *MYCN* target genes; the George_neuronal cluster, predominantly composed of *MYCN* non-amplified tumours; the George_immunogenic cluster, enrichment of immune genes; and the George_metabolic cluster, encompassing the remaining samples. A substantial portion of the George_neuronal cluster and the George_immunogenic cluster fall into subgroups 1 and 3, respectively. Specifically, 13 out of 14 samples from the George_Hi-MYCN cluster are categorized to subgroup 2 (Fig. 8h). Notably, subgroups within the George_immunogenic cluster and George_neuronal cluster also demonstrate distinct survival outcomes (Fig. 8i and j).

Califano and colleagues classified high-risk neuroblastomas into 3 main subgroups ($MYCN^{Amp}$, MYCNA), 11q-LOH (loss of heterozygosity), and mesenchymal (MES)[43]. In comparison, in the GSE85047 microarray, all cases of Califano_ MYCNA were classified in subgroup 2. Most cases in Califano_ MES or Stage1 belonged to subgroups 3 and 1 respectively (Fig. 8k). Interestingly, most cases in Califano_11q-LOH were classified in subgroup 2 (Fig. 8k), and subgroups within Califano_11q-LOH and MYCNA exhibit different survival results (Fig. 8l).

Together with other reports, our findings emphasised the extent of inner heterogeneity within the *MYCN* non-amplified population and the importance of patient stratification.

Discussion

Neuroblastoma remains a challenge in the era of personalised therapy, largely due to inter- and intra-tumoral heterogeneity. Gene amplification in *MYCN* is the first genetic marker that indicates a highly invasive, advanced neuroblastoma, which has been observed in about 20% of primary and about 40% of high-risk neuroblastoma cases[44]. Despite the extensive study of *MYCN*-amplified neuroblastomas, there is a significant unmet clinical need in *MYCN* non-amplified neuroblastomas.

In this study, using tumour expression data and ConsensusClusterPlus, we demonstrate that *MYCN* non-amplified neuroblastomas are heterogeneous and can be further classified into 3 subgroups based on their transcriptional profiling. Within them, subgroup 2 has the worst prognosis and this group exhibits a "*MYCN*" signature that is potentially induced by the overexpression of AURKA. AURKA interacts with both N-MYC and SCF (Fbxw7) ubiquitin ligase, which ubiquitinates N-MYC for degradation. Consequently, overexpression of AURKA counteracts the degradation of N-MYC, leading to the growth of neuroblastoma cells[21,45].

Subgroup 3 is accompanied by EMT and an "inflamed" phenotype, with high expression of genes related to IL2_STAT5 signaling, IL6 JAK STAT3 signaling, interferon-α activation, interferon-γ activation, and inflammatory response, consistent with the association between EMT and immune-related gene expression[46,47]. The findings were further confirmed by using CIBERSORTx deconvolution[25] to quantify various immune populations based upon a *MYCN* non-amplified neuroblastoma scRNA-seq data[26], showing increased percentages of fibroblasts, B cells, myeloid cells, T cells, and pDC (plasmacytoid dendritic cells).

The clinical implications of this subtype classification are significant, as each subtype demonstrates a unique prognosis and vulnerability to investigational therapies. For example, patients in subgroup 1 show the most favourable prognosis with a long-term survival rate above 85%, despite some of them being clinically classified as INSS stage IV or high risk. It might suggest that we should take a more careful and precise evaluation of some patients in reality after the consideration of all clinical information such as age, stage, risk status, or our stratification rather than making a decision based on a single parameter. With regard to therapy stratification, evidence showing significantly high MHC-I and CYT scores in subgroup 3 suggests that patients within this group may benefit from immunotherapy. Our analysis suggests that subgroup 3 is predicted to respond to anti-PD1 immunotherapy. The application of immunotherapy in neuroblastoma has started with treatments such as GD2 monoclonal antibody (dinutuximab) and Chimeric antigen receptor T cells (CAR-T) therapy[48,49]. Further

studies, including in *vitro*, in *vivo*, and clinical validations, are required to investigate if patients within subgroup 3 can benefit from immunotherapy.

In addition, our study suggests that patients within subgroup 2 may benefit from AURKA inhibitors that can disrupt the interaction between AURKA and N-MYC. Indeed, AURKA inhibitors, MLN8054 and MLN8237 (Alisertib), are able to disrupt this interaction, leading to N-MYC degradation and subsequently cell death and differentiation in neuroblastoma cells[45,50]. MLN8237 (Alisertib) is currently under phase 2 clinical evaluation in neuroblastoma (NCT01154816).

With the establishment of independent predictors, *MYCN* non-amplified neuroblastomas were easily classified into one of the 3 subtypes, permitting a realistic scenario in which prospective subtyping is performed in a cohort, wherein patients are assigned to different therapeutics (*e.g.*, subgroup 3 to immunotherapy, subgroup 2 to AURKA inhibitors) based on their subtype. If any one of these predictions demonstrated significant benefit, it would represent the first standard-of-care molecular biomarker selection for *MYCN* non-amplified neuroblastomas and a foundational step toward personalised therapy for this devastating disease.

Methods

Subtype identification

The study design is provided in Fig. 1a with a summary of datasets in the Supplementary Table S1. A detailed description of the approach and further characterisation of the subtypes by principal component analysis (PCA), ConsensusClusterPlus, single-sample Gene Set Enrichment Analysis (ssGSEA), weighted gene co-expression network analysis (WGCNA), and CIBERSORTx analysis is provided in the Supplementary Methods.

Analysis of hazard ratio and overall survival

The univariate and multivariate Cox proportional hazards model assessed the hazard ratio of each parameter through the survminer (v0.4.9). We performed a log-rank test to compare Kaplan-Meier survival curves between each subgroup by survival (v3.2-10). Prediction error curves of each prognostic model were generated from pec (v2019.11.03)[51].

Analysis of clinically actionable genes and drug response

To investigate subgroup-specific druggable targets, we performed an integrative analysis to assess the associations between molecular features and the response to anticancer drugs in *MYCN* non-amplified neuroblastomas. A detailed description of the approach is provided in Supplementary Methods.

Identification of independent predictors

To identify independent predictors for subgrouping, we applied a multi-cohort analysis pipeline via MetaIntegrator[30] and validated with the machine learning classifier, support vector machine (SVM) (see details in Supplementary Methods).

Tissue microarray (TMA) preparation and immunohistochemistry (IHC)

Separate a small part of the tissue specimen and shape it in a customized mold for chip production and fix it overnight in 4% paraformaldehyde (PFA). Tissue blocks were embedded in paraffin in a prepared array. Then the sample was sliced (5 μm) and adhered to a poly-L-lysine coated glass slide for immunohistochemical staining, which was performed as previously described[52,53], using specific antibody against N-MYC (1:600 dilutions; Cell Signaling Technology 51705) and Aurora kinase A (1:200 dilutions; Abcam ab52973). Blindly, with no knowledge of the clinicopathological characteristics of the tumour, the

immunoreactivity in tissue sections was observed under three microscopes at random and then evaluated by 3 pathologists. Differences in scoring were discussed until a consensus was reached. The tissue sections were then scored under an optical microscope according to the degree of staining (0 ~ 3 points were negative staining, light yellow, light brown, dark brown) and the positive range (1 ~ 4 points were 0 ~ 25%, 26 ~ 50%, 51 ~ 75%, 76 ~ 100%). Finally, samples were divided into a high-expression group and a low-expression group based on the median of the final staining score. All procedures adhered to the ethical standards set by the Clinical Committee of Xinhua Hospital, Shanghai Jiao Tong University School of Medicine (Approval No: XHEC-D-2016-037).

Code availability

Codes were implemented in R and have been deposited in GitHub: https://github.com/yz3n18/neuroblastoma.

Data availability

All data supporting the findings of the current study are listed in Supplementary Materials.

ACKNOWLEDGEMENTS

We thank all patients who participated in this study and Prof. Mark G. Jones for critical reading. For the purpose of open access, the authors have applied a CC-BY public copyright license to any Author Accepted Manuscript version arising from this submission.

AUTHOR CONTRIBUTIONS

YWang, ZW, XH, YZ conceived the research and designed the study. XH, YZ performed experiments and bioinformatics analysis. XH, YZ, YWang, ZW, CH, RME drafted the initial manuscript and performed the review and revision of the paper. XH, KC, CC, XL, PD, YG, YWu, ZL, ZW provided technical support, recruited the patients and collected clinical data. YWang, ZW supervised the study. All authors contributed to the interpretation of the results and approved the final version of the manuscript.

FUNDING

This project was supported by the UK Medical Research Council (MR/S025480/1) [YWang], the Natural Science Foundation of China (No. 81874234), Shanghai "Rising Stars of Medical Talent" Youth Development Program--Outstanding Youth Medical Talents [ZW] and the Suzhou Clinical Medicine Innovation Team Introduction Project (SZYJTD201706) [YWu]. YZ was supported by an Institute for Life Sciences PhD Studentship. CH was supported by the Gerald Kerkut Charitable Trust and the University of Southampton Central VC Scholarship Scheme.

COMPETING INTERESTS

The authors declare that they have no relevant conflict of interest.

ETHICS APPROVAL AND CONSENT TO PARTICIPATE

Sample collection for this study has been reviewed and approved by the Clinical Committee of Xinhua Hospital, Shanghai Jiao Tong University School of Medicine (Approval No: XHEC-D-2016-037). Written informed consent was obtained from all patients.

References

1. Stiller CA, Parkin DM. International variations in the incidence of neuroblastoma. *Int J Cancer* 1992; **52**(4): 538-543; e-pub ahead of print 1992/10/21; doi 10.1002/ijc.2910520407.
2. Tsubota S, Kadomatsu K. Origin and initiation mechanisms of neuroblastoma. *Cell Tissue Res* 2018; **372**(2): 211-221; e-pub ahead of print 2018/02/16; doi 10.1007/s00441-018-2796-z.
3. London WB, Castleberry RP, Matthay KK, Look AT, Seeger RC, Shimada H *et al.* Evidence for an age cutoff greater than 365 days for neuroblastoma risk group stratification in the Children's Oncology Group. *J Clin Oncol* 2005; **23**(27): 6459-6465; e-pub ahead of print 2005/08/24; doi 10.1200/jco.2005.05.571.
4. Song X, Huang C, Wang S, Yan L, Wang J, Li Y. Neck management in patients with olfactory neuroblastoma. *Oral Oncol* 2020; **101**: 104505; e-pub ahead of print 2019/12/14; doi 10.1016/j.oraloncology.2019.104505.
5. Boeva V, Louis-Brennetot C, Peltier A, Durand S, Pierre-Eugène C, Raynal V *et al.* Heterogeneity of neuroblastoma cell identity defined by transcriptional circuitries. *Nat Genet* 2017; **49**(9): 1408-1413; e-pub ahead of print 2017/07/26; doi 10.1038/ng.3921.
6. London WB, Castel V, Monclair T, Ambros PF, Pearson AD, Cohn SL *et al.* Clinical and biologic features predictive of survival after relapse of neuroblastoma: a report from the International Neuroblastoma Risk Group project. *J Clin Oncol* 2011; **29**(24): 3286-3292; e-pub ahead of print 2011/07/20; doi 10.1200/jco.2010.34.3392.
7. Cohn SL, Pearson AD, London WB, Monclair T, Ambros PF, Brodeur GM *et al.* The International Neuroblastoma Risk Group (INRG) classification system: an INRG Task Force report. *J Clin Oncol* 2009; **27**(2): 289-297; e-pub ahead of print 2008/12/03; doi 10.1200/jco.2008.16.6785.
8. Bell E, Lunec J, Tweddle DA. Cell cycle regulation targets of MYCN identified by gene expression microarrays. *Cell Cycle* 2007; **6**(10): 1249-1256; e-pub ahead of print 2007/05/15; doi 10.4161/cc.6.10.4222.
9. Kang JH, Rychahou PG, Ishola TA, Qiao J, Evers BM, Chung DH. MYCN silencing induces differentiation and apoptosis in human neuroblastoma cells. *Biochem Biophys Res Commun* 2006; **351**(1): 192-197; e-pub ahead of print 2006/10/24; doi 10.1016/j.bbrc.2006.10.020.
10. Wakamatsu Y, Watanabe Y, Nakamura H, Kondoh H. Regulation of the neural crest cell fate by N-myc: promotion of ventral migration and neuronal differentiation. *Development* 1997; **124**(10): 1953-1962; e-pub ahead of print 1997/05/01.
11. Meitar D, Crawford SE, Rademaker AW, Cohn SL. Tumor angiogenesis correlates with metastatic disease, N-myc amplification, and poor outcome in human neuroblastoma. *J Clin Oncol* 1996; **14**(2): 405-414; e-pub ahead of print 1996/02/01; doi 10.1200/jco.1996.14.2.405.
12. Goodman LA, Liu BC, Thiele CJ, Schmidt ML, Cohn SL, Yamashiro JM *et al.* Modulation of N-myc expression alters the invasiveness of neuroblastoma. *Clin Exp Metastasis* 1997; **15**(2): 130-139; e-pub ahead of print 1997/03/01; doi 10.1023/a:1018448710006.
13. Brodeur GM, Seeger RC, Schwab M, Varmus HE, Bishop JM. Amplification of N-myc in untreated human neuroblastomas correlates with advanced disease stage. *Science* 1984; **224**(4653): 1121-1124; e-pub ahead of print 1984/06/08; doi 10.1126/science.6719137.

14. Brodeur GM, Seeger RC, Schwab M, Varmus HE, Bishop JM. Amplification of N-myc sequences in primary human neuroblastomas: correlation with advanced disease stage. *Prog Clin Biol Res* 1985; **175**: 105-113; e-pub ahead of print 1985/01/01.
15. Look AT, Hayes FA, Shuster JJ, Douglass EC, Castleberry RP, Bowman LC *et al.* Clinical relevance of tumor cell ploidy and N-myc gene amplification in childhood neuroblastoma: a Pediatric Oncology Group study. *J Clin Oncol* 1991; **9**(4): 581-591; e-pub ahead of print 1991/04/01; doi 10.1200/jco.1991.9.4.581.
16. Colon NC, Chung DH. Neuroblastoma. *Adv Pediatr* 2011; **58**(1): 297-311; e-pub ahead of print 2011/07/09; doi 10.1016/j.yapd.2011.03.011.
17. Hoshida Y, Brunet JP, Tamayo P, Golub TR, Mesirov JP. Subclass mapping: identifying common subtypes in independent disease data sets. *PLoS One* 2007; **2**(11): e1195; e-pub ahead of print 2007/11/22; doi 10.1371/journal.pone.0001195.
18. Langfelder P, Horvath S. WGCNA: an R package for weighted correlation network analysis. *BMC Bioinformatics* 2008; **9**: 559; e-pub ahead of print 2008/12/31; doi 10.1186/1471-2105-9-559.
19. Valentijn LJ, Koster J, Haneveld F, Aissa RA, van Sluis P, Broekmans ME *et al.* Functional MYCN signature predicts outcome of neuroblastoma irrespective of MYCN amplification. *Proc Natl Acad Sci U S A* 2012; **109**(47): 19190-19195; e-pub ahead of print 2012/10/24; doi 10.1073/pnas.1208215109.
20. Romain C, Paul P, Kim KW, Lee S, Qiao J, Chung DH. Targeting Aurora kinase-A downregulates cell proliferation and angiogenesis in neuroblastoma. *J Pediatr Surg* 2014; **49**(1): 159-165; e-pub ahead of print 2014/01/21; doi 10.1016/j.jpedsurg.2013.09.051.
21. Otto T, Horn S, Brockmann M, Eilers U, Schüttrumpf L, Popov N *et al.* Stabilization of N-Myc is a critical function of Aurora A in human neuroblastoma. *Cancer Cell* 2009; **15**(1): 67-78; e-pub ahead of print 2008/12/30; doi 10.1016/j.ccr.2008.12.005.
22. Jin W, Zhang Y, Liu Z, Che Z, Gao M, Peng H. Exploration of the molecular characteristics of the tumor-immune interaction and the development of an individualized immune prognostic signature for neuroblastoma. *J Cell Physiol* 2021; **236**(1): 294-308; e-pub ahead of print 2020/06/09; doi 10.1002/jcp.29842.
23. Li Y, Jiang T, Zhou W, Li J, Li X, Wang Q *et al.* Pan-cancer characterization of immune-related lncRNAs identifies potential oncogenic biomarkers. *Nat Commun* 2020; **11**(1): 1000; e-pub ahead of print 2020/02/23; doi 10.1038/s41467-020-14802-2.
24. Yoshihara K, Shahmoradgoli M, Martínez E, Vegesna R, Kim H, Torres-Garcia W *et al.* Inferring tumour purity and stromal and immune cell admixture from expression data. *Nat Commun* 2013; **4**: 2612; e-pub ahead of print 2013/10/12; doi 10.1038/ncomms3612.
25. Newman AM, Liu CL, Green MR, Gentles AJ, Feng W, Xu Y *et al.* Robust enumeration of cell subsets from tissue expression profiles. *Nat Methods* 2015; **12**(5): 453-457; e-pub ahead of print 2015/03/31; doi 10.1038/nmeth.3337.
26. Dong R, Yang R, Zhan Y, Lai HD, Ye CJ, Yao XY *et al.* Single-Cell Characterization of Malignant Phenotypes and Developmental Trajectories of Adrenal Neuroblastoma. *Cancer Cell* 2020; **38**(5): 716-733.e716; e-pub ahead of print 2020/09/19; doi 10.1016/j.ccell.2020.08.014.
27. Roh W, Chen PL, Reuben A, Spencer CN, Prieto PA, Miller JP *et al.* Integrated molecular analysis of tumor biopsies on sequential CTLA-4 and PD-1 blockade reveals markers of response and resistance. *Sci Transl Med* 2017; **9**(379); e-pub ahead of print 2017/03/03; doi 10.1126/scitranslmed.aah3560.
28. Hugo W, Zaretsky JM, Sun L, Song C, Moreno BH, Hu-Lieskovan S *et al.* Genomic and Transcriptomic Features of Response to Anti-PD-1 Therapy in Metastatic

Melanoma. *Cell* 2016; **165**(1): 35-44; e-pub ahead of print 2016/03/22; doi 10.1016/j.cell.2016.02.065.

29. Su Y, Luo B, Lu Y, Wang D, Yan J, Zheng J *et al.* Anlotinib Induces a T Cell-Inflamed Tumor Microenvironment by Facilitating Vessel Normalization and Enhances the Efficacy of PD-1 Checkpoint Blockade in Neuroblastoma. *Clin Cancer Res* 2022; **28**(4): 793-809; e-pub ahead of print 2021/12/01; doi 10.1158/1078-0432.Ccr-21-2241.
30. Haynes WA, Vallania F, Liu C, Bongen E, Tomczak A, Andres-Terrè M *et al.* EMPOWERING MULTI-COHORT GENE EXPRESSION ANALYSIS TO INCREASE REPRODUCIBILITY. *Pac Symp Biocomput* 2017; **22**: 144-153; e-pub ahead of print 2016/11/30; doi 10.1142/9789813207813_0015.
31. Wang C, Gong B, Bushel PR, Thierry-Mieg J, Thierry-Mieg D, Xu J *et al.* The concordance between RNA-seq and microarray data depends on chemical treatment and transcript abundance. *Nat Biotechnol* 2014; **32**(9): 926-932; e-pub ahead of print 2014/08/26; doi 10.1038/nbt.3001.
32. Therapeutically Applicable Research to Generate Effective Treatments-phs000467. https://www.cancer.gov/ccg/research/genome-sequencing/target (2023).
33. Hartlieb SA, Sieverling L, Nadler-Holly M, Ziehm M, Toprak UH, Herrmann C *et al.* Alternative lengthening of telomeres in childhood neuroblastoma from genome to proteome. *Nat Commun* 2021; **12**(1): 1269; e-pub ahead of print 2021/02/26; doi 10.1038/s41467-021-21247-8.
34. Hagemann S, Misiak D, Bell JL, Fuchs T, Lederer MI, Bley N *et al.* IGF2BP1 induces neuroblastoma via a druggable feedforward loop with MYCN promoting 17q oncogene expression. *Mol Cancer* 2023; **22**(1): 88; e-pub ahead of print 2023/05/29; doi 10.1186/s12943-023-01792-0.
35. van Groningen T, Koster J, Valentijn LJ, Zwijnenburg DA, Akogul N, Hasselt NE *et al.* Neuroblastoma is composed of two super-enhancer-associated differentiation states. *Nat Genet* 2017; **49**(8): 1261-1266; e-pub ahead of print 2017/06/27; doi 10.1038/ng.3899.
36. Oberthuer A, Berthold F, Warnat P, Hero B, Kahlert Y, Spitz R *et al.* Customized oligonucleotide microarray gene expression-based classification of neuroblastoma patients outperforms current clinical risk stratification. *J Clin Oncol* 2006; **24**(31): 5070-5078; e-pub ahead of print 2006/11/01; doi 10.1200/jco.2006.06.1879.
37. Oberthuer A, Hero B, Berthold F, Juraeva D, Faldum A, Kahlert Y *et al.* Prognostic impact of gene expression-based classification for neuroblastoma. *J Clin Oncol* 2010; **28**(21): 3506-3515; e-pub ahead of print 2010/06/23; doi 10.1200/jco.2009.27.3367.
38. Garcia I, Mayol G, Ríos J, Domenech G, Cheung NK, Oberthuer A *et al.* A three-gene expression signature model for risk stratification of patients with neuroblastoma. *Clin Cancer Res* 2012; **18**(7): 2012-2023; e-pub ahead of print 2012/02/14; doi 10.1158/1078-0432.Ccr-11-2483.
39. Oberthuer A, Juraeva D, Hero B, Volland R, Sterz C, Schmidt R *et al.* Revised risk estimation and treatment stratification of low- and intermediate-risk neuroblastoma patients by integrating clinical and molecular prognostic markers. *Clin Cancer Res* 2015; **21**(8): 1904-1915; e-pub ahead of print 2014/09/19; doi 10.1158/1078-0432.Ccr-14-0817.
40. Rosswog C, Schmidt R, Oberthuer A, Juraeva D, Brors B, Engesser A *et al.* Molecular Classification Substitutes for the Prognostic Variables Stage, Age, and MYCN Status in Neuroblastoma Risk Assessment. *Neoplasia* 2017; **19**(12): 982-990; e-pub ahead of print 2017/11/02; doi 10.1016/j.neo.2017.09.006.

41. Gartlgruber M, Sharma AK, Quintero A, Dreidax D, Jansky S, Park Y-G *et al.* Super enhancers define regulatory subtypes and cell identity in neuroblastoma. *Nature Cancer* 2020; **2**(1): 114-128; doi 10.1038/s43018-020-00145-w.
42. Sengupta S, Das S, Crespo AC, Cornel AM, Patel AG, Mahadevan NR *et al.* Mesenchymal and adrenergic cell lineage states in neuroblastoma possess distinct immunogenic phenotypes. *Nat Cancer* 2022; **3**(10): 1228-1246; e-pub ahead of print 2022/09/23; doi 10.1038/s43018-022-00427-5.
43. Rajbhandari P, Lopez G, Capdevila C, Salvatori B, Yu J, Rodriguez-Barrueco R *et al.* Cross-Cohort Analysis Identifies a TEAD4-MYCN Positive Feedback Loop as the Core Regulatory Element of High-Risk Neuroblastoma. *Cancer Discov* 2018; **8**(5): 582-599; e-pub ahead of print 2018/03/08; doi 10.1158/2159-8290.Cd-16-0861.
44. Seeger RC, Brodeur GM, Sather H, Dalton A, Siegel SE, Wong KY *et al.* Association of multiple copies of the N-myc oncogene with rapid progression of neuroblastomas. *N Engl J Med* 1985; **313**(18): 1111-1116; e-pub ahead of print 1985/10/31; doi 10.1056/nejm198510313131802.
45. Brockmann M, Poon E, Berry T, Carstensen A, Deubzer HE, Rycak L *et al.* Small molecule inhibitors of aurora-a induce proteasomal degradation of N-myc in childhood neuroblastoma. *Cancer Cell* 2013; **24**(1): 75-89; e-pub ahead of print 2013/06/25; doi 10.1016/j.ccr.2013.05.005.
46. Terry S, Savagner P, Ortiz-Cuaran S, Mahjoubi L, Saintigny P, Thiery JP *et al.* New insights into the role of EMT in tumor immune escape. *Mol Oncol* 2017; **11**(7): 824-846; e-pub ahead of print 2017/06/15; doi 10.1002/1878-0261.12093.
47. Dongre A, Rashidian M, Reinhardt F, Bagnato A, Keckesova Z, Ploegh HL *et al.* Epithelial-to-Mesenchymal Transition Contributes to Immunosuppression in Breast Carcinomas. *Cancer Res* 2017; **77**(15): 3982-3989; e-pub ahead of print 2017/04/22; doi 10.1158/0008-5472.Can-16-3292.
48. Mujoo K, Cheresh DA, Yang HM, Reisfeld RA. Disialoganglioside GD2 on human neuroblastoma cells: target antigen for monoclonal antibody-mediated cytolysis and suppression of tumor growth. *Cancer Res* 1987; **47**(4): 1098-1104; e-pub ahead of print 1987/02/15.
49. Richards RM, Sotillo E, Majzner RG. CAR T Cell Therapy for Neuroblastoma. *Front Immunol* 2018; **9**: 2380; e-pub ahead of print 2018/11/22; doi 10.3389/fimmu.2018.02380.
50. Yang Y, Ding L, Zhou Q, Fen L, Cao Y, Sun J *et al.* Silencing of AURKA augments the antitumor efficacy of the AURKA inhibitor MLN8237 on neuroblastoma cells. *Cancer Cell Int* 2020; **20**: 9; e-pub ahead of print 2020/01/11; doi 10.1186/s12935-019-1072-y.
51. Mogensen UB, Ishwaran H, Gerds TA. Evaluating Random Forests for Survival Analysis using Prediction Error Curves. *J Stat Softw* 2012; **50**(11): 1-23; e-pub ahead of print 2012/09/01; doi 10.18637/jss.v050.i11.
52. Wang Y, Chen K, Cai Y, Cai Y, Yuan X, Wang L *et al.* Annexin A2 could enhance multidrug resistance by regulating NF-κB signaling pathway in pediatric neuroblastoma. *J Exp Clin Cancer Res* 2017; **36**(1): 111; e-pub ahead of print 2017/08/18; doi 10.1186/s13046-017-0581-6.
53. Gu Y, Lv F, Xue M, Chen K, Cheng C, Ding X *et al.* The deubiquitinating enzyme UCHL1 is a favorable prognostic marker in neuroblastoma as it promotes neuronal differentiation. *J Exp Clin Cancer Res* 2018; **37**(1): 258; e-pub ahead of print 2018/10/26; doi 10.1186/s13046-018-0931-z.

Figure Legends

Figure 1. Characterisation of molecular subtypes in the *MYCN* non-amplified neuroblastomas. (**a**) Workflow showing the study design (details provided in the Supplementary Methods). (**b**) Consensus clustering of top 50% variable genes of train cohort. (**c**) Principal component analysis (PCA) showing neuroblastoma patients with subgroup annotations.

Figure 2. Clinical characterisation of subtypes within *MYCN* non-amplified neuroblastomas identifies key distinguishing features. Graphs showing the frequency (%) of each molecular subtype in different International Neuroblastoma Staging System (INSS) stages or risk status in either train (**a**) or test (**b**) cohort. *P* values are indicated. Kaplan-Meier plots showing the overall survival in each molecular subtype or *MYCN*-amplification (*MYCN*-AMP) in either train (**c**) or test (**d**) cohort. The numbers below are n (%). P values are indicated. (**e**) Multivariate analysis of subgroup classification with risk status in *MYCN* non-amplified neuroblastomas. HR (hazard ratio), 95% CI (confidence interval), patient number (n), and *P* values are shown. (**f**) Prediction error curves (indicating a mean squared error in predicting survival status) are calculated for the subgroup (red) and INSS stage (green).

Figure 3. Defining molecular features of 3 subtypes in *MYCN* non-amplified neuroblastomas. (**a**) Heatmap showing differential expression of selected genes. Red indicates up-regulation and blue for down-regulation. Colour bars show subgroup information. (**b**) Gene set enrichment analysis (GSEA) in 3 subtypes. *FDR (false discovery rate) < 0.25; **FDR < 0.05; ***FDR < 0.01. (**c**) Weighted gene co-expression network analysis (WGCNA) showing 3 molecular modules. Nodes are colour-coded according to the WGCNA modules. Representative enriched pathway terms are indicated. (**d**) Overlay of the median-cantered $\log_2$ fold change values per subgroup on the network.

Figure 4. Subgroup 2 shows a "*MYCN*" signature, potentially induced by Aurora Kinase A overexpression. Violin plots showing *MYCN* mRNA levels (**a**) or *MYCN* scores (**b**) in neuroblastomas. *P* values are indicated. (**c**) Multivariate analysis of *MYCN* score and risk status in *MYCN* non-amplified neuroblastomas. HR (hazard ratio), 95% CI (confidence interval), patient number (n), and *P* values are shown. (**d**) Protein-protein interaction (PPI) network showing an interaction between AURKA and MYCN. (**e**) Violin plot showing *AURKA* mRNA

levels in neuroblastomas. *P* values are indicated. (**f**) Kaplan-Meier plot showing the overall survival in samples with low *vs.* high *AURKA* expression. The numbers below are n (%). HR (hazard ratio), 95% CI (confidence interval), patient number (n), and *P* values are shown.

Figure 5. N-MYC expression correlates with Aurora kinase A status in *MYCN* non-amplified neuroblastomas and is indicative of patient survival. (**a**) Representative N-MYC staining pattern (negative or positive N-MYC) in *MYCN* non-amplified neuroblastoma tissue microarray cores. Scale bar: 1mm (the left column) and 50μm (the right column). (**b**) Kaplan-Meier plot showing the overall survival in samples with negative *vs.* positive N-MYC expression. The numbers below are n (%). HR (hazard ratio), 95% CI (confidence interval), patient number (n), and *P* values are shown. (**c**) Adjacent tumour sections from representative cases showing N-MYC and Aurora Kinase A expression in *MYCN* non-amplified neuroblastoma. Scale bars: 50μm. (**d**) Kaplan-Meier plot showing the overall survival in samples with low *vs.* high Aurora kinase A expression. The numbers below are n (%). HR (hazard ratio), 95% CI (confidence interval), patient number (n), and *P* values are shown. (**e**) Graph showing percentage (%) and numbers of samples with low or high Aurora kinase A in the negative or positive N-MYC group. $P = 0.041$.

Figure 6. Subgroup 3 is accompanied by an "inflamed" gene signature. (**a**) Heatmap showing neuroblastoma-associated immune pathways and immune cell signatures in subgroups and *MYCN*-AMP. Graphs showing the cumulative distribution of CYT (**b**) or MHC-1 (**c**) scores in different subgroups and *MYCN*-AMP. (**d**) Violin plots showing immune scores in different subgroups and *MYCN*-AMP in train, test, or train plus test cohort. (**e**) Graph showing cell compositions of each subgroup using CIBERSORTx analysis. (**f**) Graph showing differential putative immunotherapeutic response in different subgroups. Bonferroni adjusted *P* values indicated. (**g**) Subclass association (SA) matrix for the comparison between different subgroups and vehicle/anlotinib treated mouse. Bonferroni adjusted *P* values indicated.

Figure 7. Identification and evaluation of independent predictors to subgroup patients within *MYCN* non-amplified neuroblastomas. (**a**) Predicted probability of each subgroup in 5 different cohorts. Each dot in the scatter plot corresponds to a sample (x-axis: predicted probability of subgroup 2, y-axis: predicted probability of subgroup 3). The histogram plot above the scatter plot displayed the distribution of subgroup 2 probabilities while the plot to the right of the scatter plot displayed the distribution of subgroup 3 probabilities. (**b**) Kaplan-

Meier plots showing the overall survival in predicted molecular subtype in 5 different cohorts. The numbers below are n (%). *P* values are indicated. (**c**) Prediction differences in the superseries GSE47792 using data from either RNA-seq (GSE49711) or microarray (GSE49710).

Figure 8. A systematic comparison of the subgroup classifier with previously published gene expression classifiers. (**a**) Prediction differences in GSE16476 using the subgrouping method from this report (named Hu) or Valentijn and colleagues (Valentijn). (**b**) Multivariate analysis of subgroup classification with Valentijn classification in *MYCN* non-amplified neuroblastomas. HR (hazard ratio), 95% CI (confidence interval), patient number (n), and *P* values are shown. (**c**) Prediction differences in E-MTAB-1781 using the subgrouping method from this report (named Hu) or Oberthuer and colleagues (Oberthuer's svm_th24). (**d**) Multivariate analysis of subgroup classification with Oberthuer's svm_th24 classification in *MYCN* non-amplified neuroblastomas. HR (hazard ratio), 95% CI (confidence interval), patient number (n), and *P* values are shown. (**e**) Prediction differences in GSE49711 using the subgrouping method from this report (named Hu) or Westermann and colleagues (Westermann). Kaplan-Meier plots showing the overall survival in Westermann_MNA-HR (**f**) or Westermann_MNA-LR (**g**) patients using the subgrouping method from this report. Numbers below are n (%). P values are indicated. (**h**) Prediction differences in GSE49711 using subgrouping method from this report (named Hu) or George and colleagues (George). Kaplan-Meier plots showing the overall survival in George_Immunogenic (**i**) or George_Neuronal (**j**) patients using the subgrouping method from this report. The numbers below are n (%). *P* values are indicated. (**k**) Prediction differences in GSE85047 using the subgrouping method from this report (named Hu) or Califano and colleagues (Califano). (**l**) Kaplan-Meier plots showing the overall survival in Califano_11q-LOH & MYCNA patients using the subgrouping method from this report. The numbers below are n (%). *P* values are indicated.

707

Figure 1

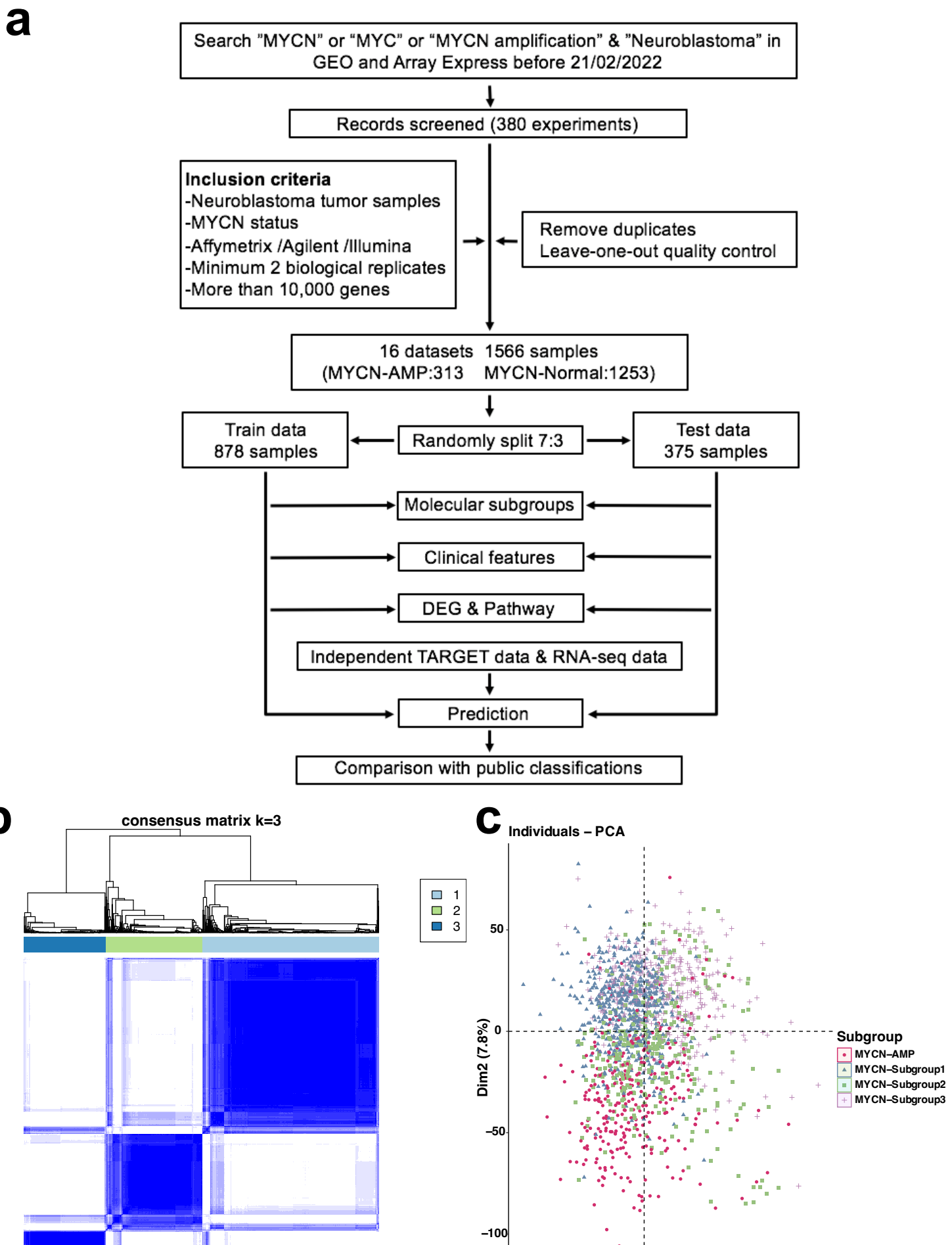
a
Search "MYCN" or "MYC" or "MYCN amplification" & "Neuroblastoma" in GEO and Array Express before 21/02/2022
Records screened (380 experiments)
Inclusion criteria
-Neuroblastoma tumor samples
-MYCN status
-Affymetrix /Agilent /Illumina
-Minimum 2 biological replicates
-More than 10,000 genes
Remove duplicates
Leave-one-out quality control
16 datasets 1566 samples
(MYCN-AMP:313 MYCN-Normal:1253)
Train data
878 samples
Randomly split 7:3
Test data
375 samples
Molecular subgroups
Clinical features
DEG & Pathway
Independent TARGET data & RNA-seq data
Prediction
Comparison with public classifications
b
consensus matrix k=3
1
2
3
c
Individuals – PCA
Dim2 (7.8%)
Dim1 (10%)
50
0
−50
−100
−100
0
100
Subgroup
MYCN−AMP
MYCN−Subgroup1
MYCN−Subgroup2
MYCN−Subgroup3

Figure 2

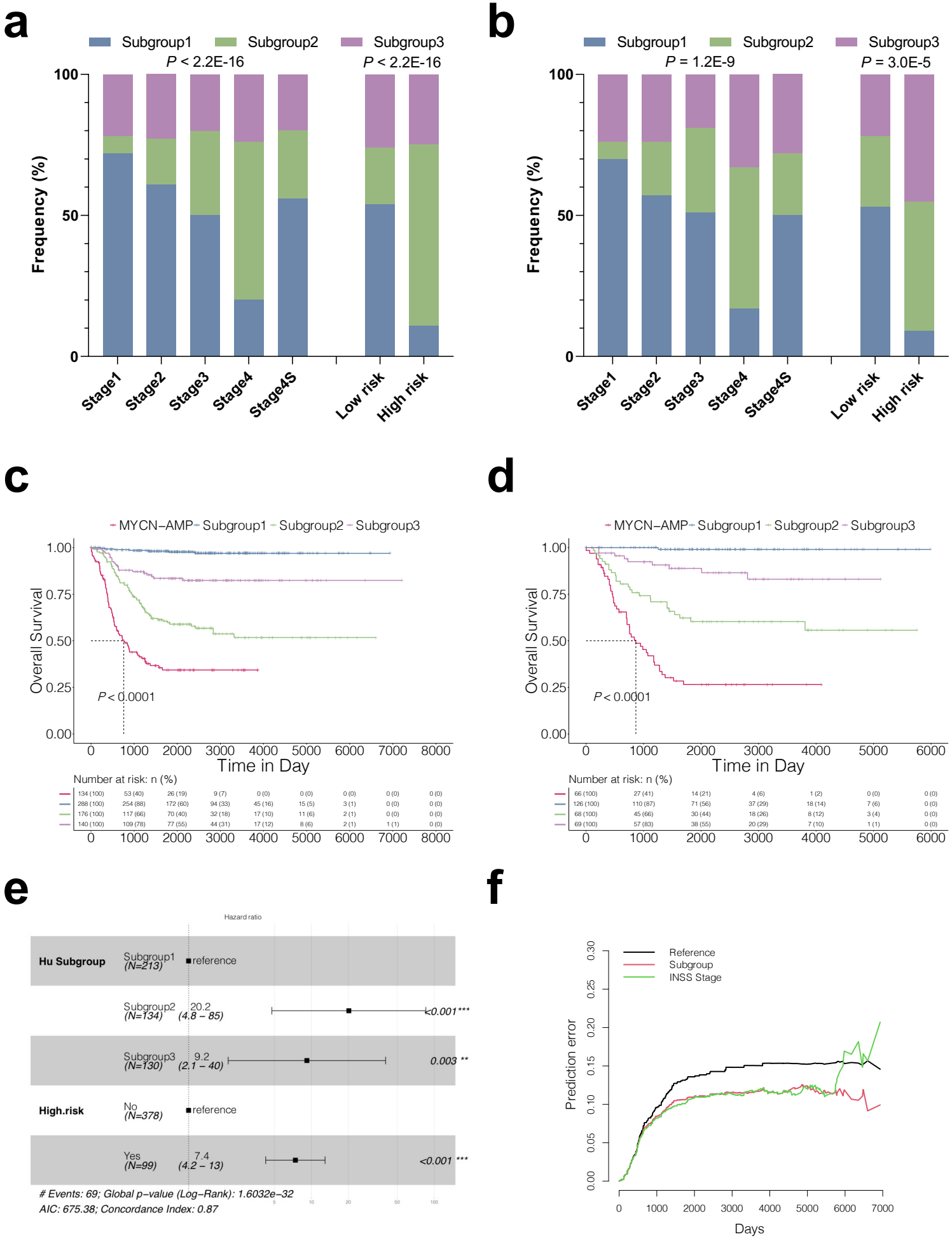
a
Subgroup1
Subgroup2
Subgroup3
P < 2.2E-16
P < 2.2E-16
Frequency (%)
100
50
0
Stage1
Stage2
Stage3
Stage4
Stage4S
Low risk
High risk
b
Subgroup1
Subgroup2
Subgroup3
P = 1.2E-9
P = 3.0E-5
Frequency (%)
100
50
0
Stage1
Stage2
Stage3
Stage4
Stage4S
Low risk
High risk
c
MYCN−AMP
Subgroup1
Subgroup2
Subgroup3
Overall Survival
1.00
0.75
0.50
0.25
0.00
P < 0.0001
0
1000
2000
3000
4000
5000
6000
7000
8000
Time in Day
Number at risk: n (%)
134 (100) 53 (40) 26 (19) 9 (7) 0 (0) 0 (0) 0 (0) 0 (0) 0 (0)
288 (100) 254 (88) 172 (60) 94 (33) 45 (16) 15 (5) 3 (1) 0 (0) 0 (0)
176 (100) 117 (66) 70 (40) 32 (18) 17 (10) 11 (6) 2 (1) 0 (0) 0 (0)
140 (100) 109 (78) 77 (55) 44 (31) 17 (12) 8 (6) 2 (1) 1 (1) 0 (0)
0
1000
2000
3000
4000
5000
6000
7000
8000
d
MYCN−AMP
Subgroup1
Subgroup2
Subgroup3
Overall Survival
1.00
0.75
0.50
0.25
0.00
P < 0.0001
0
1000
2000
3000
4000
5000
6000
Time in Day
Number at risk: n (%)
66 (100) 27 (41) 14 (21) 4 (6) 1 (2) 0 (0) 0 (0)
126 (100) 110 (87) 71 (56) 37 (29) 18 (14) 7 (6) 0 (0)
68 (100) 45 (66) 30 (44) 18 (26) 8 (12) 3 (4) 0 (0)
69 (100) 57 (83) 38 (55) 20 (29) 7 (10) 1 (1) 0 (0)
0
1000
2000
3000
4000
5000
6000
e
Hazard ratio
Hu Subgroup
Subgroup1 (N=213)
reference
Subgroup2 (N=134)
20.2 (4.8 – 85)
<0.001***
Subgroup3 (N=130)
9.2 (2.1 – 40)
0.003 **
High.risk
No (N=378)
reference
Yes (N=99)
7.4 (4.2 – 13)
<0.001 ***
Events: 69; Global p−value (Log−Rank): 1.6032e−32
AIC: 675.38; Concordance Index: 0.87
5
10
20
50
100
f
Reference
Subgroup
INSS Stage
Prediction error
0.00
0.05
0.10
0.15
0.20
0.25
0.30
0
1000
2000
3000
4000
5000
6000
7000
Days

Figure 3

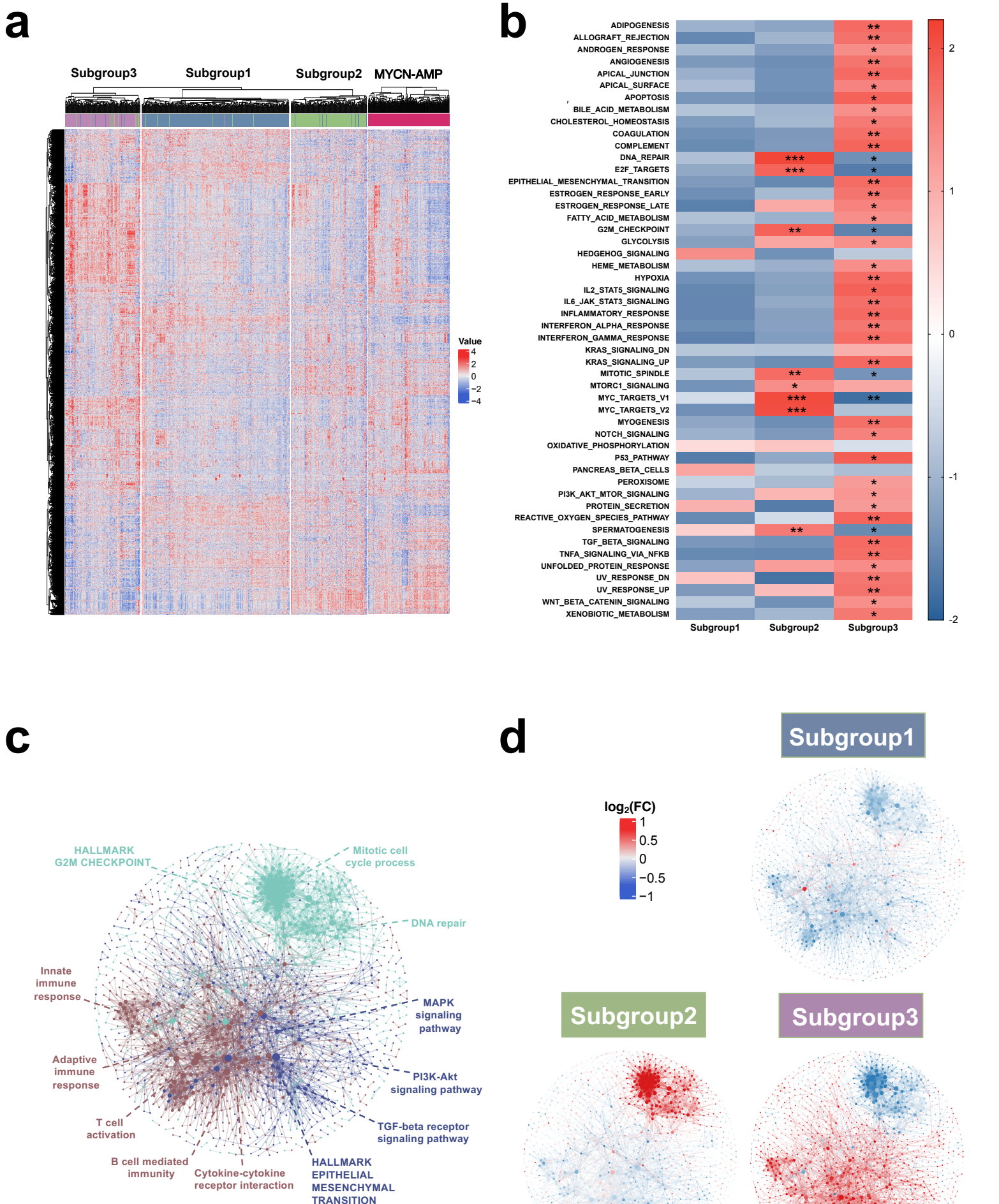
a
Subgroup3
Subgroup1
Subgroup2
MYCN-AMP
Value
4
2
0
−2
−4
b
ADIPOGENESIS
ALLOGRAFT_REJECTION
ANDROGEN_RESPONSE
ANGIOGENESIS
APICAL_JUNCTION
APICAL_SURFACE
APOPTOSIS
BILE_ACID_METABOLISM
CHOLESTEROL_HOMEOSTASIS
COAGULATION
COMPLEMENT
DNA_REPAIR
E2F_TARGETS
EPITHELIAL_MESENCHYMAL_TRANSITION
ESTROGEN_RESPONSE_EARLY
ESTROGEN_RESPONSE_LATE
FATTY_ACID_METABOLISM
G2M_CHECKPOINT
GLYCOLYSIS
HEDGEHOG_SIGNALING
HEME_METABOLISM
HYPOXIA
IL2_STAT5_SIGNALING
IL6_JAK_STAT3_SIGNALING
INFLAMMATORY_RESPONSE
INTERFERON_ALPHA_RESPONSE
INTERFERON_GAMMA_RESPONSE
KRAS_SIGNALING_DN
KRAS_SIGNALING_UP
MITOTIC_SPINDLE
MTORC1_SIGNALING
MYC_TARGETS_V1
MYC_TARGETS_V2
MYOGENESIS
NOTCH_SIGNALING
OXIDATIVE_PHOSPHORYLATION
P53_PATHWAY
PANCREAS_BETA_CELLS
PEROXISOME
PI3K_AKT_MTOR_SIGNALING
PROTEIN_SECRETION
REACTIVE_OXYGEN_SPECIES_PATHWAY
SPERMATOGENESIS
TGF_BETA_SIGNALING
TNFA_SIGNALING_VIA_NFKB
UNFOLDED_PROTEIN_RESPONSE
UV_RESPONSE_DN
UV_RESPONSE_UP
WNT_BETA_CATENIN_SIGNALING
XENOBIOTIC_METABOLISM
Subgroup1
Subgroup2
Subgroup3
2
1
0
-1
-2
c
HALLMARK G2M CHECKPOINT
Mitotic cell cycle process
DNA repair
Innate immune response
MAPK signaling pathway
Adaptive immune response
PI3K-Akt signaling pathway
T cell activation
TGF-beta receptor signaling pathway
B cell mediated immunity
Cytokine-cytokine receptor interaction
HALLMARK EPITHELIAL MESENCHYMAL TRANSITION
d
log2(FC)
1
0.5
0
−0.5
−1
Subgroup1
Subgroup2
Subgroup3

Figure 4

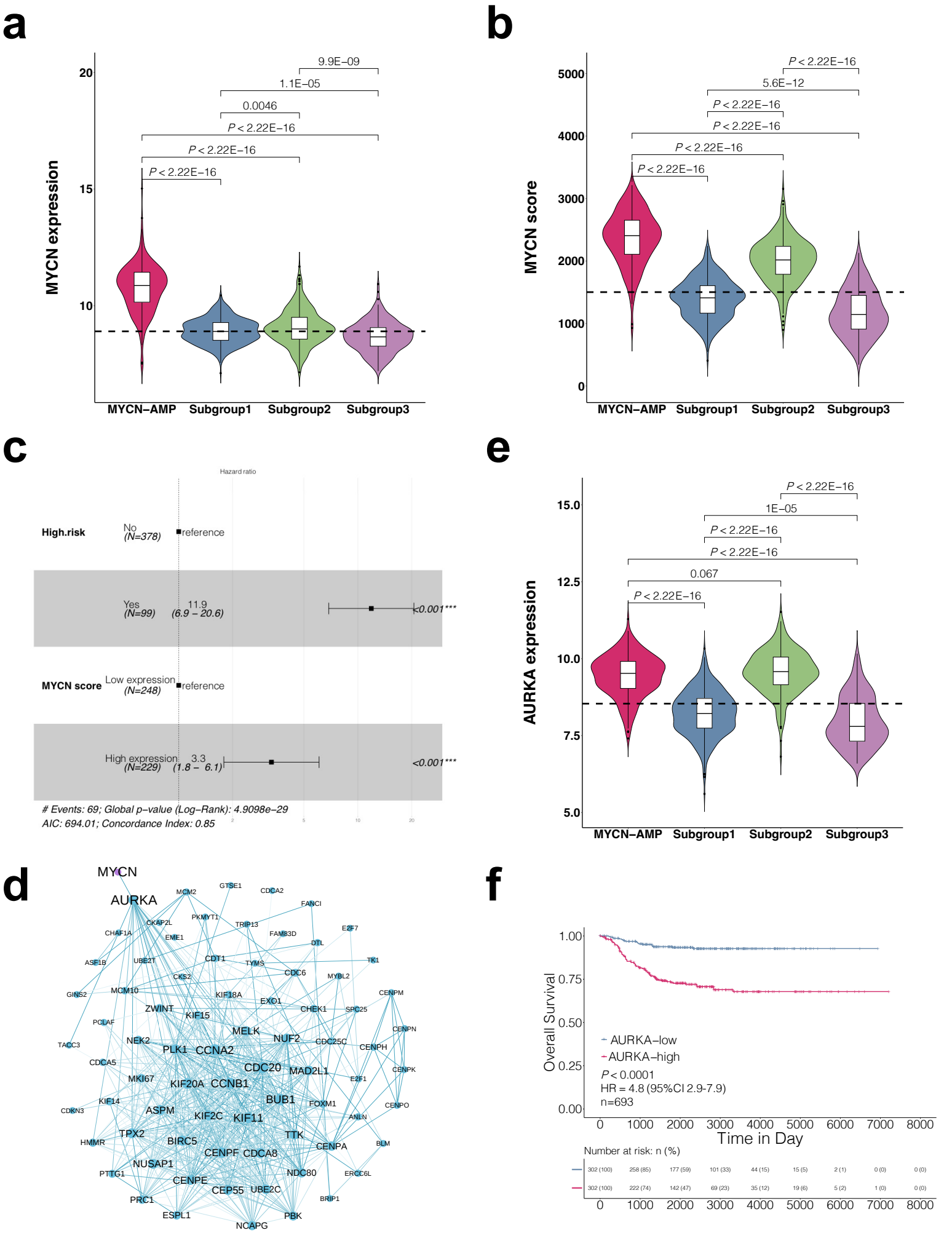
a
MYCN expression
20
15
10
9.9E−09
1.1E−05
0.0046
P < 2.22E−16
P < 2.22E−16
P < 2.22E−16
MYCN−AMP
Subgroup1
Subgroup2
Subgroup3
b
MYCN score
5000
4000
3000
2000
1000
0
P < 2.22E−16
5.6E−12
P < 2.22E−16
P < 2.22E−16
P < 2.22E−16
P < 2.22E−16
MYCN−AMP
Subgroup1
Subgroup2
Subgroup3
c
Hazard ratio
High.risk
No (N=378) reference
Yes (N=99) 11.9 (6.9 – 20.6) <0.001***
MYCN score
Low expression (N=248) reference
High expression (N=229) 3.3 (1.8 – 6.1) <0.001***
Events: 69; Global p−value (Log−Rank): 4.9098e−29
AIC: 694.01; Concordance Index: 0.85
e
AURKA expression
15.0
12.5
10.0
7.5
5.0
P < 2.22E−16
1E−05
P < 2.22E−16
P < 2.22E−16
0.067
P < 2.22E−16
MYCN−AMP
Subgroup1
Subgroup2
Subgroup3
d
MYCN
AURKA
MCM2
GTSE1
CDCA2
FANCI
CKAP2L
PKMYT1
TRIP13
CHAF1A
EME1
FAM83D
E2F7
DTL
ASF1B
UBE2T
CDT1
TYMS
TK1
CKS2
CDC6
MYBL2
GINS2
MCM10
KIF18A
EXO1
CENPM
ZWINT
KIF15
CHEK1
SPC25
PCLAF
MELK
NUF2
CENPN
TACC3
NEK2
PLK1
CCNA2
CDC25C
CENPH
CDCA5
CDC20
MAD2L1
CENPK
MKI67
KIF20A
CCNB1
E2F1
KIF14
BUB1
FOXM1
CENPO
CDKN3
ASPM
KIF2C
KIF11
ANLN
TPX2
TTK
HMMR
BIRC5
CENPA
BLM
CENPF
CDCA8
NUSAP1
PTTG1
NDC80
ERCC6L
CENPE
CEP55
UBE2C
BRIP1
PRC1
ESPL1
PBK
NCAPG
f
Overall Survival
1.00
0.75
0.50
0.25
0.00
AURKA−low
AURKA−high
P < 0.0001
HR = 4.8 (95%CI 2.9-7.9)
n=693
0
1000
2000
3000
4000
5000
6000
7000
8000
Time in Day
Number at risk: n (%)
302 (100) 258 (85) 177 (59) 101 (33) 44 (15) 15 (5) 2 (1) 0 (0) 0 (0)
302 (100) 222 (74) 142 (47) 69 (23) 35 (12) 19 (6) 5 (2) 1 (0) 0 (0)
0
1000
2000
3000
4000
5000
6000
7000
8000

Figure 5

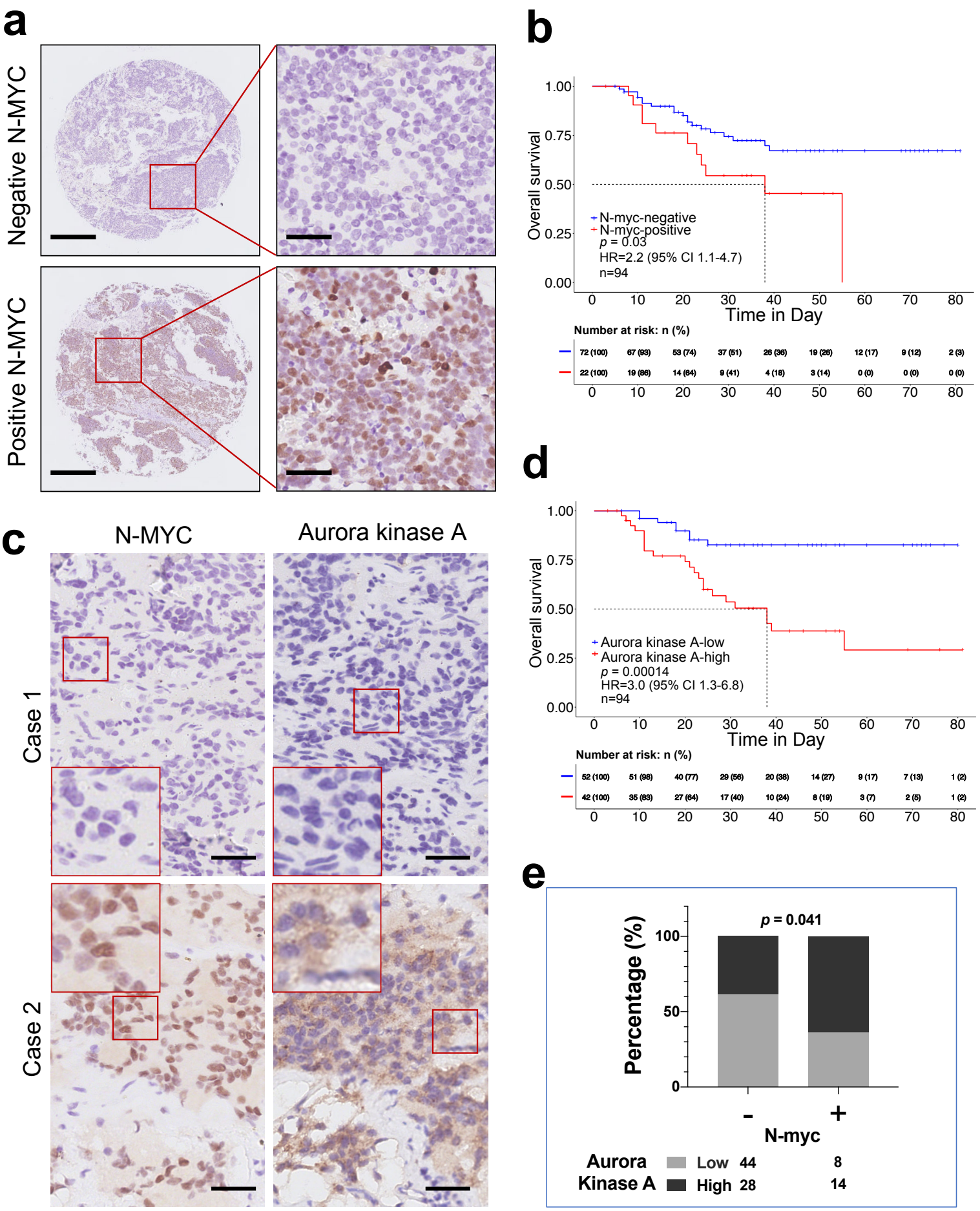
a
Negative N-MYC
Positive N-MYC
b
Overall survival
1.00
0.75
0.50
0.25
0.00
N-myc-negative
N-myc-positive
p = 0.03
HR=2.2 (95% CI 1.1-4.7)
n=94
0 10 20 30 40 50 60 70 80
Time in Day
Number at risk: n (%)
72 (100) 67 (93) 53 (74) 37 (51) 26 (36) 19 (26) 12 (17) 9 (12) 2 (3)
22 (100) 19 (86) 14 (64) 9 (41) 4 (18) 3 (14) 0 (0) 0 (0) 0 (0)
c
N-MYC
Aurora kinase A
Case 1
Case 2
d
Overall survival
1.00
0.75
0.50
0.25
0.00
Aurora kinase A-low
Aurora kinase A-high
p = 0.00014
HR=3.0 (95% CI 1.3-6.8)
n=94
0 10 20 30 40 50 60 70 80
Time in Day
Number at risk: n (%)
52 (100) 51 (98) 40 (77) 29 (56) 20 (38) 14 (27) 9 (17) 7 (13) 1 (2)
42 (100) 35 (83) 27 (64) 17 (40) 10 (24) 8 (19) 3 (7) 2 (5) 1 (2)
e
p = 0.041
Percentage (%)
100
50
0
-
+
N-myc
Aurora Kinase A
Low 44 8
High 28 14

Figure 6

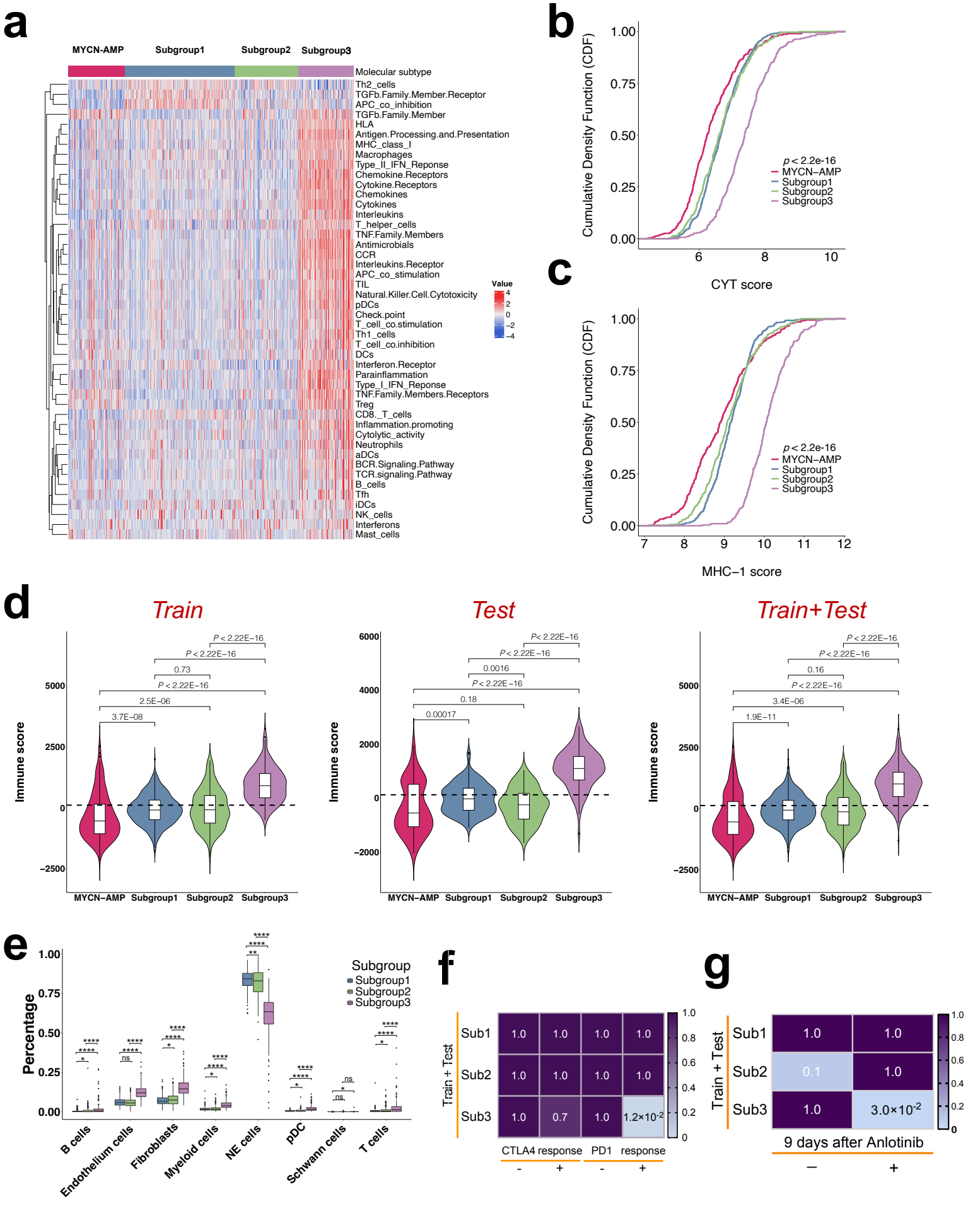
a
MYCN-AMP
Subgroup1
Subgroup2
Subgroup3
Molecular subtype
Th2_cells
TGFb.Family.Member.Receptor
APC_co_inhibition
TGFb.Family.Member
HLA
Antigen.Processing.and.Presentation
MHC_class_I
Macrophages
Type_II_IFN_Reponse
Chemokine.Receptors
Cytokine.Receptors
Chemokines
Cytokines
Interleukins
T_helper_cells
TNF.Family.Members
Antimicrobials
CCR
Interleukins.Receptor
APC_co_stimulation
TIL
Natural.Killer.Cell.Cytotoxicity
pDCs
Check.point
T_cell_co.stimulation
Th1_cells
T_cell_co.inhibition
DCs
Interferon.Receptor
Parainflammation
Type_I_IFN_Reponse
TNF.Family.Members.Receptors
Treg
CD8._T_cells
Inflammation.promoting
Cytolytic_activity
Neutrophils
aDCs
BCR.Signaling.Pathway
TCR.signaling.Pathway
B_cells
Tfh
iDCs
NK_cells
Interferons
Mast_cells
Value
4
2
0
−2
−4
b
Cumulative Density Function (CDF)
1.00
0.75
0.50
0.25
0.00
6
8
10
CYT score
p < 2.2e-16
MYCN−AMP
Subgroup1
Subgroup2
Subgroup3
c
Cumulative Density Function (CDF)
1.00
0.75
0.50
0.25
0.00
7
8
9
10
11
12
MHC−1 score
p < 2.2e-16
MYCN−AMP
Subgroup1
Subgroup2
Subgroup3
d
Train
Test
Train+Test
Immune score
P < 2.22E−16
P < 2.22E−16
0.73
P < 2.22E−16
2.5E−06
3.7E−08
5000
2500
0
−2500
MYCN−AMP
Subgroup1
Subgroup2
Subgroup3
Immune score
P < 2.22E−16
P < 2.22E−16
0.0016
P < 2.22E−16
0.18
0.00017
6000
4000
2000
0
−2000
MYCN−AMP
Subgroup1
Subgroup2
Subgroup3
Immune score
P < 2.22E−16
P < 2.22E−16
0.16
P < 2.22E−16
3.4E−06
1.9E−11
5000
2500
0
−2500
MYCN−AMP
Subgroup1
Subgroup2
Subgroup3
e
Percentage
1.00
0.75
0.50
0.25
0.00
Subgroup
Subgroup1
Subgroup2
Subgroup3
B cells
Endothelium cells
Fibroblasts
Myeloid cells
NE cells
pDC
Schwann cells
T cells
f
Train + Test
Sub1
Sub2
Sub3
1.0
1.0
1.0
1.0
1.0
1.0
1.0
1.0
1.0
0.7
1.0
1.2×10-2
1.0
0.8
0.6
0.4
0.2
0
CTLA4 response
PD1 response
-
+
-
+
g
Train + Test
Sub1
Sub2
Sub3
1.0
1.0
0.1
1.0
1.0
3.0×10-2
1.0
0.8
0.6
0.4
0.2
0
9 days after Anlotinib
−
+

Figure 7

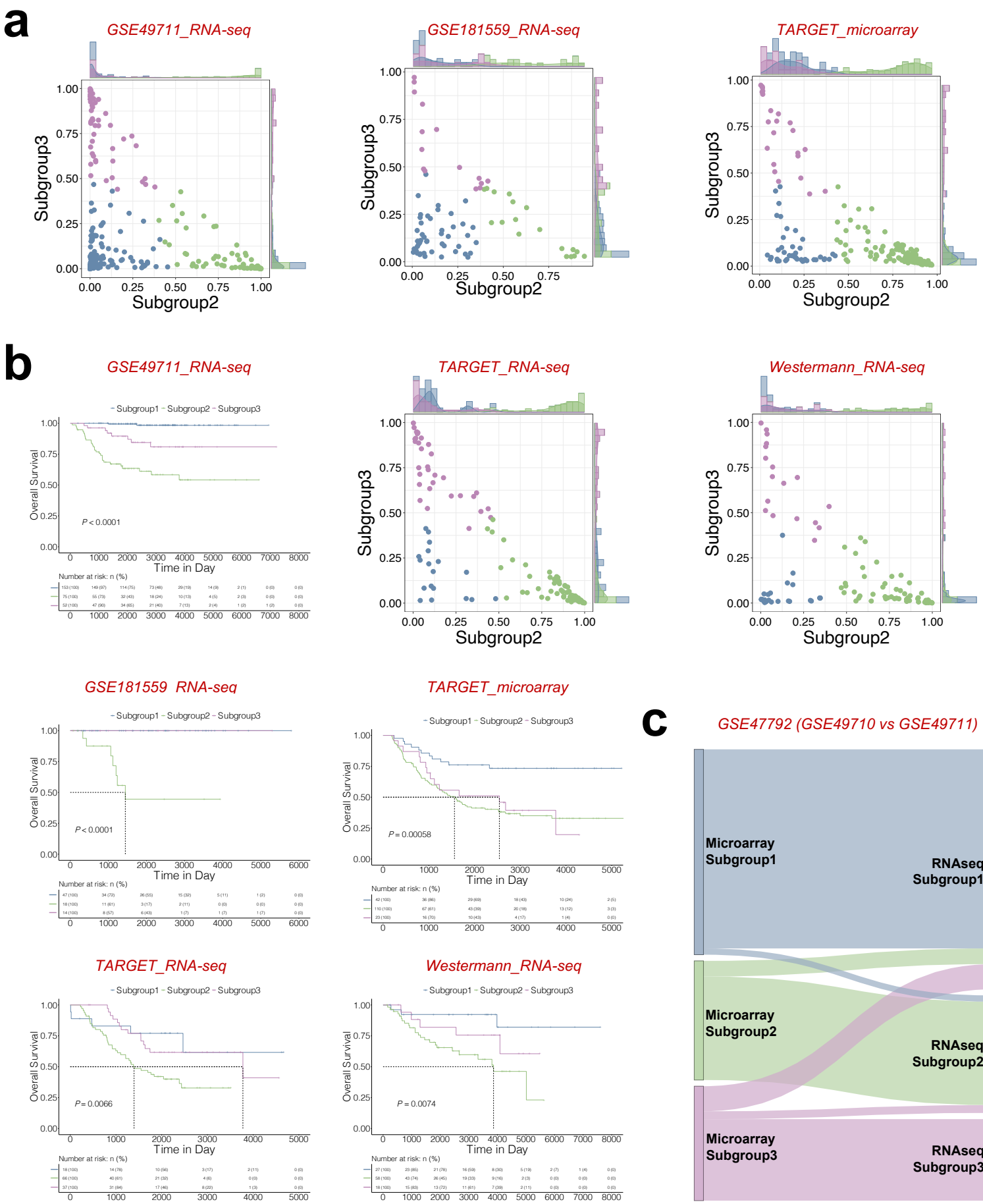
a
GSE49711_RNA-seq
GSE181559_RNA-seq
TARGET_microarray
Subgroup3
Subgroup2
b
GSE49711_RNA-seq
TARGET_RNA-seq
Westermann_RNA-seq
Subgroup1 Subgroup2 Subgroup3
Overall Survival
P < 0.0001
Time in Day
Number at risk: n (%)
GSE181559_RNA-seq
TARGET_microarray
P = 0.00058
TARGET_RNA-seq
Westermann_RNA-seq
P = 0.0066
P = 0.0074
c
GSE47792 (GSE49710 vs GSE49711)
Microarray Subgroup1
Microarray Subgroup2
Microarray Subgroup3
RNAseq Subgroup1
RNAseq Subgroup2
RNAseq Subgroup3

Figure 8

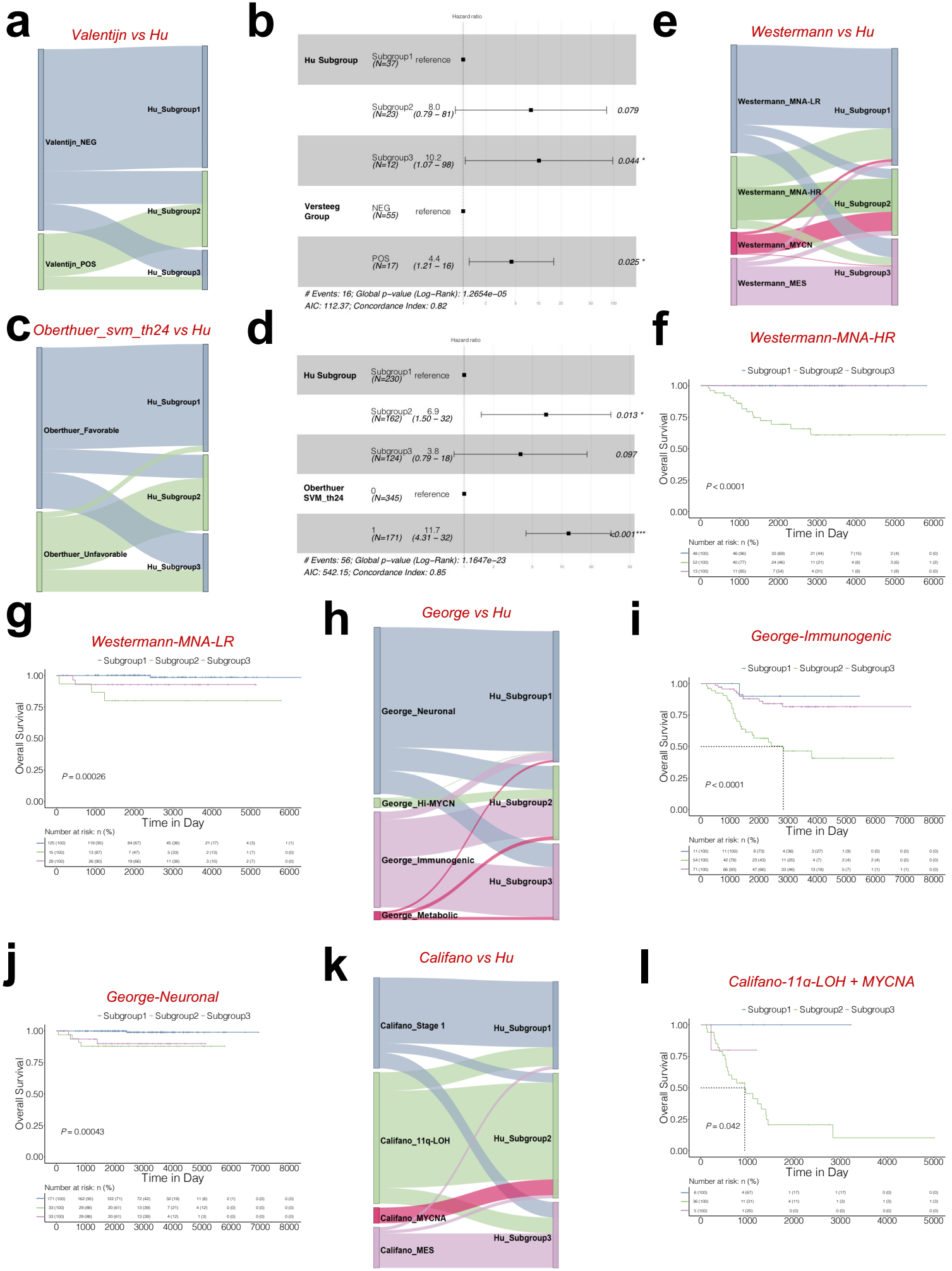
a
Valentijn vs Hu
Valentijn_NEG
Valentijn_POS
Hu_Subgroup1
Hu_Subgroup2
Hu_Subgroup3
b
Hazard ratio
Hu Subgroup
Subgroup1 (N=37) reference
Subgroup2 (N=23) 8.0 (0.79 – 81) 0.079
Subgroup3 (N=12) 10.2 (1.07 – 98) 0.044 *
Versteeg Group
NEG (N=55) reference
POS (N=17) 4.4 (1.21 – 16) 0.025 *
Events: 16; Global p–value (Log–Rank): 1.2654e–05
AIC: 112.37; Concordance Index: 0.82
e
Westermann vs Hu
Westermann_MNA-LR
Westermann_MNA-HR
Westermann_MYCN
Westermann_MES
Hu_Subgroup1
Hu_Subgroup2
Hu_Subgroup3
c
Oberthuer_svm_th24 vs Hu
Oberthuer_Favorable
Oberthuer_Unfavorable
Hu_Subgroup1
Hu_Subgroup2
Hu_Subgroup3
d
Hazard ratio
Hu Subgroup
Subgroup1 (N=230) reference
Subgroup2 (N=162) 6.9 (1.50 – 32) 0.013 *
Subgroup3 (N=124) 3.8 (0.79 – 18) 0.097
Oberthuer SVM_th24
0 (N=345) reference
1 (N=171) 11.7 (4.31 – 32) <0.001***
Events: 56; Global p–value (Log–Rank): 1.1647e–23
AIC: 542.15; Concordance Index: 0.85
f
Westermann-MNA-HR
Subgroup1 Subgroup2 Subgroup3
Overall Survival
P < 0.0001
Time in Day
Number at risk: n (%)
g
Westermann-MNA-LR
Subgroup1 Subgroup2 Subgroup3
Overall Survival
P = 0.00026
Time in Day
Number at risk: n (%)
h
George vs Hu
George_Neuronal
George_Hi-MYCN
George_Immunogenic
George_Metabolic
Hu_Subgroup1
Hu_Subgroup2
Hu_Subgroup3
i
George-Immunogenic
Subgroup1 Subgroup2 Subgroup3
Overall Survival
P < 0.0001
Time in Day
Number at risk: n (%)
j
George-Neuronal
Subgroup1 Subgroup2 Subgroup3
Overall Survival
P = 0.00043
Time in Day
Number at risk: n (%)
k
Califano vs Hu
Califano_Stage 1
Califano_11q-LOH
Califano_MYCNA
Califano_MES
Hu_Subgroup1
Hu_Subgroup2
Hu_Subgroup3
l
Califano-11q-LOH + MYCNA
Subgroup1 Subgroup2 Subgroup3
Overall Survival
P = 0.042
Time in Day
Number at risk: n (%)